

P-Glycoprotein Substrate Binding Domains Are Located at the Transmembrane Domain/Transmembrane Domain Interfaces: A Combined Photoaffinity Labeling-Protein Homology Modeling Approach

Karin Pleban, Stephan Kopp, Edina Csaszar, Michael Peer, Thomas Hrebicek, Andreas Rizzi, Gerhard F. Ecker, and Peter Chiba

Institute of Medical Chemistry (K.P., S.K., M.P., P.C.), Medical University of Vienna, Department of Pharmaceutical Chemistry (K.P., G.F.E.), Institute of Analytical Chemistry (T.H., A.R.), and the Mass Spectrometry Facility, Max F. Perutz Laboratories, University Departments at the Vienna Biocenter (E.C.), University of Vienna, Vienna, Austria

Received September 6, 2004; accepted October 27, 2004

ABSTRACT

P-glycoprotein (P-gp) is an energy-dependent multidrug efflux pump conferring resistance to cancer chemotherapy. Characterization of the mechanism of drug transport at a molecular level represents an important prerequisite for the design of pump inhibitors, which resensitize cancer cells to standard chemotherapy. In addition, P-glycoprotein plays an important role for early absorption, distribution, metabolism, excretion, and toxicity profiling in drug development. A set of propafenone-type substrate photoaffinity ligands has been used in this study in conjunction with matrix-assisted laser desorption/ionization time-of-flight mass spectrometry to define the substrate binding domain(s) of P-gp in more detail. The highest labeling was observed in transmembrane segments 3, 5, 8, and 11. A homology model

for P-gp was generated on the basis of the dimeric crystal structure of *Vibrio cholerae* MsbA, an essential lipid transporter. Thereafter, the labeling pattern was projected onto the 3D atomic-detail model of P-gp to allow a visualization of the binding domain(s). Labeling is predicted by the model to occur at the two transmembrane domain/transmembrane domain interfaces formed between the amino- and carboxyl-terminal half of P-gp. These interfaces are formed by transmembrane (TM) segments 3 and 11 on one hand and TM segments 5 and 8 on the other hand. Available data on LmrA and AcrB, two bacterial multidrug efflux pumps, suggest that binding at domain interfaces may be a general feature of polyspecific drug efflux pumps.

Multidrug resistance represents a serious obstacle to successful cancer chemotherapy. Although multifactorial in etiology, one type of multidrug resistance is associated with the overexpression of energy-dependent membrane-bound pumps, which intercept and efflux drugs before they reach their intracellular target structures. P-glycoprotein (ABCB1) represents a paradigm ATP-dependent efflux pump expressed in human cancer cells. In addition to its expression in cancer cells, P-gp is also physiologically expressed in a number of tissues such as intestinal epithelial cells, at the brush

border of renal tubule epithelial cells, the canalicular side of hepatocytes, and in capillary endothelial cells forming the blood-brain barrier. It thus interferes with oral drug absorption and drug delivery to the brain, and it enhances renal and biliary excretion. P-gp has therefore attracted considerable attention as a nontarget in the field of drug development, because for a large number of active compounds, interaction with P-glycoprotein might compromise their future development into a drug. Considerable energy has therefore been devoted to the characterization of molecular features that make compounds P-gp substrates and to the definition of the molecular mechanism of drug transport by P-gp. A number of studies have dealt with the kinetics and thermodynamics of the transport process (Senior and Gadsby 1997; Sauna and Ambudkar, 2000, 2001; Al-Shawi et al., 2003). In addition, site-directed mutagenesis has been used to replace individual

This work was supported by grants from the Austrian Science Fund (grant 17014-B11) and the Austrian National Bank (grant 10654).

The coordinates of the P-gp model are available from the authors upon request.

Article, publication date, and citation information can be found at <http://molpharm.aspetjournals.org>.
doi:10.1124/mol.104.006973.

ABBREVIATIONS: P-gp, P-glycoprotein; ABC, ATP binding cassette; TMD, transmembrane domain; NBD, nucleotide binding domain; TM, transmembrane segment; MALDI-TOF, matrix-assisted laser desorption/ionization time of flight; Vc, *Vibrio cholerae*; TFA, trifluoroacetic acid; CHCA, α -cyano-4-hydroxycinnamic acid; AA, amino acid.

amino acid residues and characterize mutant P-gp with respect to ATPase activity, substrate binding, and transport characteristics (Hafkemeyer et al., 1998; Loo and Clarke, 2004a,b). P-gp has been overexpressed, purified, and reconstituted successfully to obtain biological material for structural resolution of the transporter. This endeavor has resulted in low-resolution structures obtained by electron cryomicroscopy (Rosenberg et al., 2001, 2003). Nevertheless, an atomic detail structure of P-gp or of any other ATP-dependent multidrug transporter is not available to date. Photoaffinity labeling studies have identified regions that are accessible for substrates (Peer et al., 2004). Atomic details of the substrate binding domain and of the dynamics of the transport process, however, still remain elusive.

In the present study, a set of substrate photoaffinity ligands related to the lead compound propafenone were used to photolabel P-gp. After gel electrophoretic separation and in-gel proteolytic degradation of the P-gp band, ligand-labeled peptides were identified by matrix-assisted laser desorption/ionization time-of-flight (MALDI-TOF) mass spectrometry. A homology model for P-gp was established using the essential lipid transporter MsbA from *Vibrio cholerae* as a template. The information obtained by photoaffinity-labeling studies was projected onto this model indicating two pseudosymmetric binding domains formed by TM segments 3 and 11 (corresponding to TM segment 3 of the N-terminal and TM5 of the C-terminal TMD) on one hand and TMs 5 and 8 (corresponding to TM segment 5 of the N-terminal and TM2 of the C-terminal half of P-gp) on the other hand. Data indicate that the initial binding of substrates occurs at the TMD/TMD interfaces. A reconciliation of the model with cross-linking data of double-cysteine mutants has been possible. Data indicate that entry of substrates via the TMD/TMD interface might represent a common property of multidrug efflux pumps.

Materials and Methods

Design and Synthesis of Compounds. The design and synthesis of propafenone-type photoaffinity ligands has been described previously (Ecker et al., 2002). Structures were confirmed by infrared, mass spectrometry, NMR spectroscopy, and elemental analysis and are shown in Table 1.

Cell Lines. Insect Sf9 cells were obtained from the American Type Culture Collection (Manassas, VA).

Preparation of Plasma Membrane Vesicles. Plasma membrane preparations of Sf9 cells transfected with the baculovirus construct containing the His-tagged *mdr1* gene (Germann et al., 1990) were prepared by nitrogen cavitation and subsequent discontinuous sucrose-gradient centrifugation as described previously (Schmid et al., 1999).

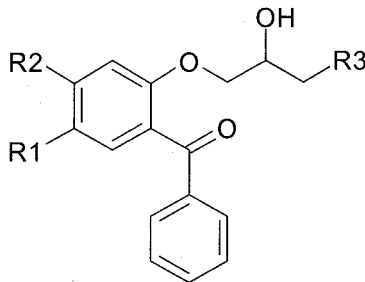
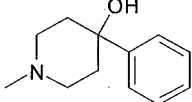
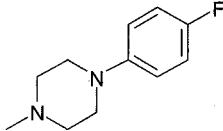
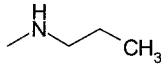
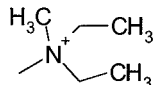
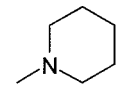
Photolabeling of P-gp and Gel Electrophoretic Separation Conditions. Plasma membrane-vesicles were taken up in 50 mM Tris-HCl, pH 7.4, and preincubated with ligand at a concentration of 10 nM. Samples were preincubated at room temperature for 15 min. Thereafter, samples were placed on ice and irradiated intermittently with a 500 W mercury lamp (Lot-Oriel, Darmstadt, Germany) for 6 × 30 s in the presence of the photoactivatable propafenones. Control samples were irradiated in the absence of photoligands. A 1-mm glass plate was placed in the light path to filter most of the UV light with wavelengths lower than 300 nm. After irradiation, samples were centrifuged at 50,000g for 30 min at 4°C. Protein pellets (30 µg of total plasma membrane protein per lane) were taken up in 1× SDS sample buffer, loaded onto a 10% polyacrylamide gel, and run at 35

mA for 60 min using a Hoefer Mighty Small II SE250 unit (Amersham Biosciences Inc., Piscataway, NJ). Gels were fixed in methanol/glacial acetic acid/water (50:10:40) for 30 min and washed overnight in double-distilled water. Bands were visualized by silver staining as described previously (Ecker et al., 2002), and the P-gp band was excised and subjected to in-gel digestion as described below.

Chemicals for In-Gel Digestion and Mass Spectrometry. High-quality water for the in-gel digestion and the mass spectrometric experiments was prepared using a Milli-Q water purification system (Millipore Corporation, Billerica, MA). Ammonium hydrogen carbonate was obtained from Fluka (Vienna, Austria), dithiothreitol for the reduction of proteins before in-gel digestion was purchased from Serva (Heidelberg, Germany), iodoacetamide was supplied by Sigma-Aldrich (Vienna, Austria), and chymotrypsin was obtained from Roche Diagnostics GmbH (sequencing grade; Mannheim, Germany). Acetone was from AppliChem (Darmstadt, Germany); acetonitrile, methanol, and isopropanol were purchased from Sigma-Aldrich (high-performance liquid chromatography grade); trifluoroacetic acid (TFA) was obtained from Pierce (Rockford, IL); and formic acid was supplied by VWR (Darmstadt, Germany). The α -cyano-4-hydroxycinnamic acid (CHCA) matrix for the MALDI-TOF measurements was purchased from Bruker Daltonik GmbH (Bremen, Germany) and used without further purification. Nitrocellulose was purchased from Bio-Rad (Hercules, CA). Protein and peptide standards used to calibrate the MALDI mass spectrometer were obtained from Bruker. In-gel digestions were performed according to the procedure described by Ecker et al. (2002).

TABLE 1

Chemical structure and exact mass of benzophenone-type photoligands

| Compound | R1 | R2 | R3 | Exact Mass |
|----------|------------------|-------------------|---|------------|
| GPV 51 | H | H |  | 327.183 |
| GPV 317 | H | H |  | 431.210 |
| GPV 319 | H | H |  | 434.200 |
| GPV 442 | -CH ₃ | H |  | 327.183 |
| GPV 708 | H | H |  | 342.210 |
| BP 11 | H | -OCH ₃ |  | 369.194 |

MALDI-TOF Mass Spectrometry. A Bruker REFLEX III MALDI-TOF instrument, equipped with a standard nitrogen laser (337 nm) was used for mass spectrometry. The spectra were recorded in reflectron mode, positive ionization, and with an acceleration voltage of 25 kV. The laser power was varied on a relative scale of 0 to 100 and was kept at the threshold value to obtain appropriate signal intensity. The calibration of the instrument was done externally. Samples were prepared with a 75:25 (v/v) mixture of CHCA matrix (saturated solution in acetone) and nitrocellulose [10 mg/ml solution in acetone/isopropanol, 50:50 (v/v)]. A 1- μ l aliquot of the mixture was placed onto the sample slide and allowed to dry at room temperature. In-gel digested P-gp (0.5 μ l) was mixed with 0.5 μ l 0.1% TFA on this thin layer of matrix crystals and vacuum-dried. Samples were washed with ice-cold 0.1% TFA. Hydrophobic peptides were purified and concentrated on Poros 20 R1 material (Applied Biosystems, Foster City, CA) loaded into GeLoader tips (Eppendorf-Netheler-Hinz GmbH, Hamburg, Germany). The chromatography material was conditioned with 0.1% TFA, and the peptides were eluted with CHCA matrix [saturated solution in 0.1% TFA/acetonitrile 50:50 (v/v)] directly onto the sample slide. Each spectrum was produced by accumulating data from 90 to 120 consecutive laser shots. Spectra were interpreted with the aid of the Mascot (Matrix Science Ltd., London, UK) or MS-Fit (Clauser et al., 1999) software using the nonredundant database (National Center for Biotechnology Information Resources, National Institutes of Health, Bethesda, MD). Ligand-modified masses were matched to peptide masses generated by *in silico* digests of the protein with the aid of a custom program developed in our laboratory.

Data Analysis. Statistical analysis was performed using the unpaired Student's *t* test with a 95% confidence interval for the sample mean.

Generation of a Protein Homology Model of P-gp Using Vc-MsbA as Template. Primary sequences of the proteins are deposited in the Swiss-Prot TrEMBL database (<http://au.expasy.org/sprot/>) with the accession numbers P08183 (P-gp), Q03518 (TAP1), and Q9KQW9 (Vc-MsbA). Crystal structures were obtained from the Brookhaven Protein DataBank (<http://www.rcsb.org/pdb/>). Sequence alignments were generated in InsightII, release 2000 (Accelrys, San Diego, CA) implemented on a Silicon Graphics Octane R12000 workstation. A geometric validation of the 3D model was carried out using the ProStat/Structure Check and/or Verify3D modules in InsightII. Minimization at splice points was performed using the CHARMM force field (Accelrys). Graphics were generated in MOE (Chemical Computing Group, Cologne, Germany) and visual molecular dynamics (Humphrey et al., 1996).

To identify putative transmembrane helices we initially submitted the N- and C-terminal halves of P-gp to the MPEx membrane protein explorer (<http://blanco.biomol.uci.edu/mpex>). Thereafter, the N- and C-terminal halves of P-gp (1–614 and 697–1280) were aligned with Vc-MsbA separately. Amino acids 1 to 33 and the six C-terminal amino acids were not considered in the model because they have no counterpart in MsbA. In addition, the linker region extending from amino acid positions 629 to 697 was deleted from the sequence, because evidence for a functional relevance of this protein sequence is lacking (Seigneuret et al., 2003). The alignment was performed using the Blosum62 matrix with a gap penalty of 11 and a gap extension penalty of 1, yielding an alignment identical with that suggested previously by Chang (2003). This alignment was carefully checked to avoid deletions or insertions in conserved regions and in transmembrane helices and, if necessary, corrected manually. The sequences corresponding to the intracellular loops 2 and 4 (AA250–284 and AA893–927) were not considered in the homology model because they are not resolved in the Vc-MsbA crystal structure, indicating the highly flexible nature of this loop (Chang, 2003). Finally, the homology model was minimized at splice points with 500 cycles of steepest descent algorithm followed by 550 cycles of conjugate gradient minimization. For final model assembly, the N- and

C-terminal P-gp halves were superimposed onto Vc-MsbA and merged.

In addition to the three full-length crystal structures of bacterial ABC transporters, the X-ray structures of a number of nucleotide binding domains (NBDs) of other ABC transporters are available. These structures suggest that the NBD conformation observed in Vc-MsbA is a result of crystallization conditions and probably does not represent a physiologically relevant conformation. Therefore, we decided to model the NBDs on the basis of the crystal structure of TAP1, which in this domain shows highest sequence homology with P-gp. The NBD model for P-gp was obtained according to the procedure described in detail for LmrA (Ecker et al., 2004). Sequences of the N- and C-terminal NBD were aligned separately using the Blosum 62 matrix with a gap penalty of 11 and a gap extension penalty of 1. The alignment was manually refined to avoid deletions and/or insertions in conserved regions. The models were again minimized at splice points with a cycle of 500 steps of steepest descent algorithm minimization.

Generation of the P-gp model was therefore performed in three steps: in the first step, a model of the TMDs and the NBDs was generated using Vc-MsbA as template. In the second step, an alternate NBD model was generated, which, in a third step, replaced the Vc-MsbA-type NBDs according to a method published previously for the bacterial transporter LmrA (Ecker et al., 2004). The quality of the models was assessed by a ProStat structure check, indicating that 98% of the residues were in allowed regions of the Ramachandran plot.

Cross-linking data and low-resolution electron microscopy studies suggest that the transmembrane domains of P-gp form a funnel-shaped pore that is closer at its cytoplasmic end than at the extracellular surface. Because the model presented in Fig. 5 (model A) shows an inverted funnel-shaped pore, we created an alternate model by rotating the two TMD domains of P-gp about a point located at the leaflet interface. Subsequent repositioning of the NBDs and recalculation of the TMD-NBD linker regions gave the final model (model B), shown in Fig. 6. Both models conform to most but not all distance constraints obtained by cysteine cross-linking data. Distances in our model seem to be similar to those obtained in a previously published P-gp model (Stenham et al., 2003) (Table 2).

Results

Propafenones Are Substrates of P-Glycoprotein.

Propafenone analogs have previously been shown to be accumulated in inside-out plasma membrane vesicles in an ATP-dependent and cyclosporine A-inhibitable manner (Schmid et al., 1999). A net flux of compounds was only measurable when the compounds carried a permanent positive charge at the nitrogen atom. In contrast, compounds with a tertiary nitrogen atom diffuse through membranes quickly, and thus a net flux of these compounds is not detectable (Schmid et al., 1999). However, similar to quaternary compounds, propafenone analogs containing a tertiary nitrogen atom caused a shift in fluorescence when P-gp was reacted with the conformation-sensitive antibody UIC2 (S. Park and P. Chiba, unpublished observations). In addition, a number of studies from our group demonstrated that propafenones inhibit the transport of known P-gp substrates, including rhodamine 123, daunorubicin (Chiba et al., 1995; Ecker et al., 1999, 2002), mitoxantrone, and vinblastine (S. Kopp and P. Chiba, unpublished observations). Photolabeling of plasma-membrane vesicles with the radioactive analog [³H]GPV51 was demonstrated to be highly specific for P-gp, and other plasma membrane proteins were not labeled to any significant extent. In addition, nonradioactive GPV51 competed with bind-

TABLE 2

Distances of residues in the models that have previously been shown to be cross-linked in double cysteine mutants TM helix a and TM helix b denote the pairs of putative transmembrane α -helices in which cross-links between two cysteines introduced at residues a and b could be obtained

The source reference is given in the rightmost column. To allow a more convenient identification of the mutated residues, they are denoted with their original (nonmutated) three-letter amino acid code followed by the position in the primary sequence. All distances are minimum distances and are measured between the C_α atoms of the specified residues. In instances in which more than one pair of residues has been cross-linked, the superscripts 1 to 4 are used to identify these pairs, and the minimum and maximum distances are given. In the case of the triple-cysteine mutants (Stenham et al., 2003), the minimum distance is given.

| TM Helix a | Residue a | TM Helix b | Residue b | X-Link Distance | Distance Model A Å | Distance Model B | Reference |
|------------|---|------------|---|-----------------|-----------------------|------------------|----------------------------|
| 2 | Tyr117-Ser119 | 11 | Gly955-Phe957 | 12 | 12 | 17 | Stenham et al., 2003 |
| 2 | Val133 ¹ , Cys137 ² | 11 | Ala935 ¹ , Gly939 ² | 7 | 18–26 | 15–25 | Loo et al., 2004b |
| 4 | Ser222 | 10 | Ile868, Gly872 | 9–25 | 40–41 | 40–41 | Loo and Clarke, 2001 |
| 4 | Leu227, Val231–Ala233, Ile235, Leu236 | 11 | Ser993 | 7 | 28–31 | 22–25 | Loo and Clarke, 2000 |
| 5 | Gly317–Thr319 | 8 | Asn753-Phe755 | 11 | 12 | 16 | Stenham et al., 2003 |
| 5 | Asn296 ¹ , Ile299 ^{2,3} , Gly300 ⁴ | 8 | Gly774 ^{1,3} , Phe770 ^{2,4} | 7 | 15–19 | 15–21 | Loo et al., 2004a |
| 5 | Ile306 | 10 | Ile868, Gly872 | 13–25 | 24–25 | 20–21 | Loo and Clarke, 2001 |
| 5 | Ile306 | 11 | Thr945 | 13–25 | 28 | 22 | Loo and Clarke, 2001 |
| 5 | Ile306 ¹ , Ala295 ² , Ile299 ² | 12 | Val982 ¹ , Gly984 ¹ , Ser993 ² | 7–25 | 20–29 | 10–22 | Loo and Clarke, 2000, 2001 |
| 6 | Leu339, Pro350 | 10 | Ile868, Gly872, Val874-Met876 | 7–25 | 28–33 | 23–31 | Loo and Clarke, 2000, 2001 |
| 6 | Leu339, Pro350 | 11 | Phe942, Thr945, Gly939 | 7–25 | 20–29 | 9–22 | Loo and Clarke, 2000, 2001 |
| 6 | Leu339 ¹ , Phe343 ² , Gly346 ³ , Pro350 ⁴ | 12 | Val982 ¹ , Ala985 ¹ , Met986 ² , Gly989 ³ , Ser993 ⁴ | 7–25 | 18–32 | 10–27 | Loo and Clarke, 2000, 2001 |

ing of [³H]GPV51 in a concentration-dependent manner (Ecker et al., 2002).

Identification of Substrate-Binding Domains of P-gp. P-gp was overexpressed in Sf9 insect cells using a baculovirus expression system (Germann et al., 1990). Plasma membrane vesicles were prepared from these cells by nitrogen cavitation and labeled with propafenone-type photoligands. Structures of these photoaffinity ligands are shown in Table 1. As shown previously, these benzophenone-type ligands exhibited an unchanged quantitative structure-activity relationship compared with parental phenylpropionophenones (Ecker et al., 2002). Upon irradiation, compounds are photoactivated in the carbonyl group, which represents a pharmacophoric substructure of these compounds (Ecker et al., 2002). After irradiation, membrane proteins were separated by SDS-polyacrylamide gel electrophoresis, and the bands were visualized by silver staining. The 140-kD protein corresponding to core glycosylated P-gp was excised and proteolytically degraded in gel by chymotrypsin digestion. The ensuing peptide fragments were eluted from the gel and identified by high-resolution MALDI-TOF mass spectrometry. Because the efficiency of the photochemical reaction is low, the majority of peaks in the mass spectrum corresponded to unmodified peptide fragments and allowed assessment of the coverage of the sequence with unmodified peptide fragments. The α -helical TM segments of the TMDs, which are considered to be responsible for solute binding and translocation, were in their entirety represented by ligand-unmodified peptide fragments. Overall, the sequence coverage in the TMDs exceeded 95%, whereas that in the NBD was approximately 80%. Mass peaks were assigned to P-gp by comparison with a list of theoretical peptide masses obtained by in silico proteolytic degradation of the protein with chymotrypsin. Because chymotrypsin recognition sites are frequent in TM segments, experiments were performed under incomplete digest conditions. This prevented loss of sequence coverage in protein regions with clustered protease-recognition sites. Under these conditions, up to seven missing cleavage sites were observed, and thus in silico digest files were generated using this information.

Ligand-modified peptide fragments were assigned after subtracting the exact mass of the ligand. As evidence accumulated that more than one ligand can be adopted in binding pockets of multispecific proteins at the same time (Neyfakh, 2002; Yu et al., 2002), binding of more than one ligand to the same peptide fragment was also considered. Indeed, a number of masses were candidate peaks for fragments modified by two ligands. These peptides were included in the frequency distribution analysis shown below.

Six ligands of different mass were used for the experiments to improve the signal-to-noise ratio. The rationale of these experiments was as follows: peptide fragments that are covalently modified by the photoligand shift from their original position in the mass spectrum to an m/z , which is increased by the ligand mass. Because only a small fraction of the peptides is photochemically modified, two peaks are then detected, one at an m/z corresponding to the unmodified peptide and one with an m/z corresponding to the sum of the masses of the peptide fragment and the ligand. With a certain albeit low probability, this peak might be assigned incorrectly. Use of ligands with different mass and determination of consensus binding regions, however, minimizes any

potential influence of incorrect peak assignments. We did not attempt to use other classes of photoactivatable compounds, because quantitative structure-activity relationship studies for these ligands are not available.

The number of fragments containing a particular amino acid was determined and plotted as a function of this amino acid position as described in Ecker et al. (2004). The resulting frequency-distribution analysis of photolabeling is shown in Fig. 1. Predicted TM segments are shown in magenta. The remainder of the sequence is shown in black. Benzophenone-type ligands have initially been reported to be nonselective (Dorman and Prestwich, 2000). A preferred reaction with methionine residues in proteins has been reported (Rihakova et al., 2002; Wahlstrom et al., 2002). Methionine residues in Fig. 1 were therefore highlighted in red. Indeed, a number of methionine residues were identified to be located in peaks (Met197, Met440, Met701, Met791, Met969, and Met1027) or close to peaks of the trace (Met68, Met69, Met105, Met111, Met796, Met948, and Met949). This indicates that the frequency distribution analysis of Fig. 1 correctly reflects the preference of the photochemical reaction. However, it is important to note that not all peaks contain methionine residues, which is in agreement with the ability of benzophenones to react with aliphatic residues (Dorman and Prestwich, 2000). For example, predicted TM segments 5 and 8 are strongly labeled but do not contain methionine residues. Figure 1 also shows that the presence of a methionine residue is not a sufficient precondition for reaction with the photoligands, because a number of methionine residues are not labeled (Met89, Met192, Met450, Met497, Met878, and Met1010). These residues are thus inaccessible for the photoligands.

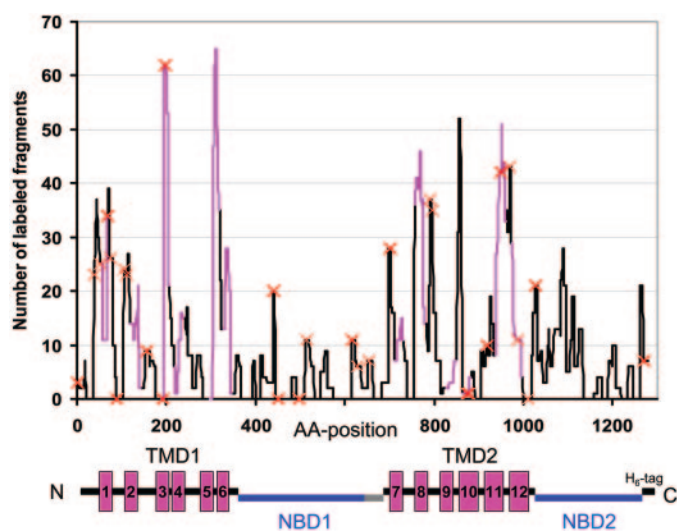


Fig. 1. Frequency distribution analysis of labeled peptide fragments. The number of labeled fragments in which each particular amino acid residue in the primary sequence of P-gp is found is plotted as a function of this amino acid position. The positions of putative TM segments are shown in magenta, and the remainder of the sequence is in black. A schematic representation below the graph allows easier orientation. TMDs 1 and 2 represent the N-terminal and C-terminal transmembrane domains, respectively, and the motor domains NBD1 and NBD2 are shown in blue. The linker region is indicated in gray, and the C-terminal hexa-His tag is depicted in black. The positions of methionine residues are highlighted by red symbols (x). The highest labeling is observed for putative TMs 3, 5, 8, and 11. In addition, the loop region connecting TMs 9 and 10 (extracellular loop 5) has a high labeling score.

Inspection of Fig. 1 indicates four major sites of labeling within predicted TM segments. These are putative TMs 3 and 5 in the N-terminal half and TM segments 8 and 11 in the C-terminal half of P-gp. Strong labeling is also detected in the loop region connecting TM segments 9 and 10. Minor labeling is observed N- and C-terminal of predicted TM1, N-terminal of TM2, in putative TM6, at the N terminus of putative TM7, and C-terminal of TM8. The methionine residue Met969, which is located in the loop region connecting TMs 11 and 12 (extracellular loop 6), is located in the tip of a small riding peak C-terminal of the strongly labeled TM11. According to the P-gp models presented in detail below (Figs. 5 and 6), these sites of minor labeling, as well as the strongly labeled loop region between TMs 9 and 10, are located close to the predicted extra- and intracellular membrane-water interfaces. Because the affinity ligands are expected to electrostatically interact with phosphate head groups of the membrane phospholipids in protonated form, this labeling at the membrane surface did not come as a surprise. However, these sites were scattered and only had in common their position at the respective membrane-water interfaces. Labeling at these positions, which lie outside the predicted transmembrane segments, is thus unlikely to be related to substrate transport.

Peak areas in Fig. 1 provide a measure of the density of labeled peptide fragments found in a particular protein region and were thus used to further discriminate between regions of high and low labeling. Peak areas were expressed as the sum of those amino acid residues in ligand-modified fragments, which overlapped with the respective TM segment. Data are presented for each of the six photoligands individually to show the reproducibility of the results. To decrease the influence of surface-labeled residues (by protrusion of labeled fragments from loops into TM segments), the three most N-terminal and C-terminal amino acid residues of each predicted TM helix were excluded from calculation. Figure 2, A through F, represents data for each of the six photoaffinity ligands, respectively. For ligands GPV51, GPV317, GPV319, GPV442, and BP11, the highest labeling was invariably observed for putative TM segments 3, 5, 8, and 11, indicating that these four TM segments are involved in the initial substrate-binding event in nonenergized P-gp (i.e., in the absence of ATP). For the quaternary compound GPV708, which carries a permanent positive charge at the nitrogen atom, labeling was only observed in putative TMs 3 and 11, whereas TM segments 5 and 8 were not labeled (Fig. 2F). This was an initial indication for a pairwise contribution of TMs 3/11 and 5/8 to substrate binding.

Figure 3 shows a composite representation of peak area data for all six ligands. The average percentage of labeling in the respective TM segment was calculated as a percentage of labeling in all TM segments. TM segments 3, 5, 8, and 11 were clearly responsible for nearly 70% of total labeling.

The probability of detection of labeled peptide fragments within a particular protein region might depend on the recovery of peptide fragments from the same protein region. To evaluate a potential influence of this variable on the photolabeling results, the expected retrieval of peptide fragments from individual TM segments was determined, based on *in silico* digests. Results are shown in Fig. 4. The experimentally determined average photolabeling (as shown in Fig. 3) was plotted as a function of the expected coverage of individ-

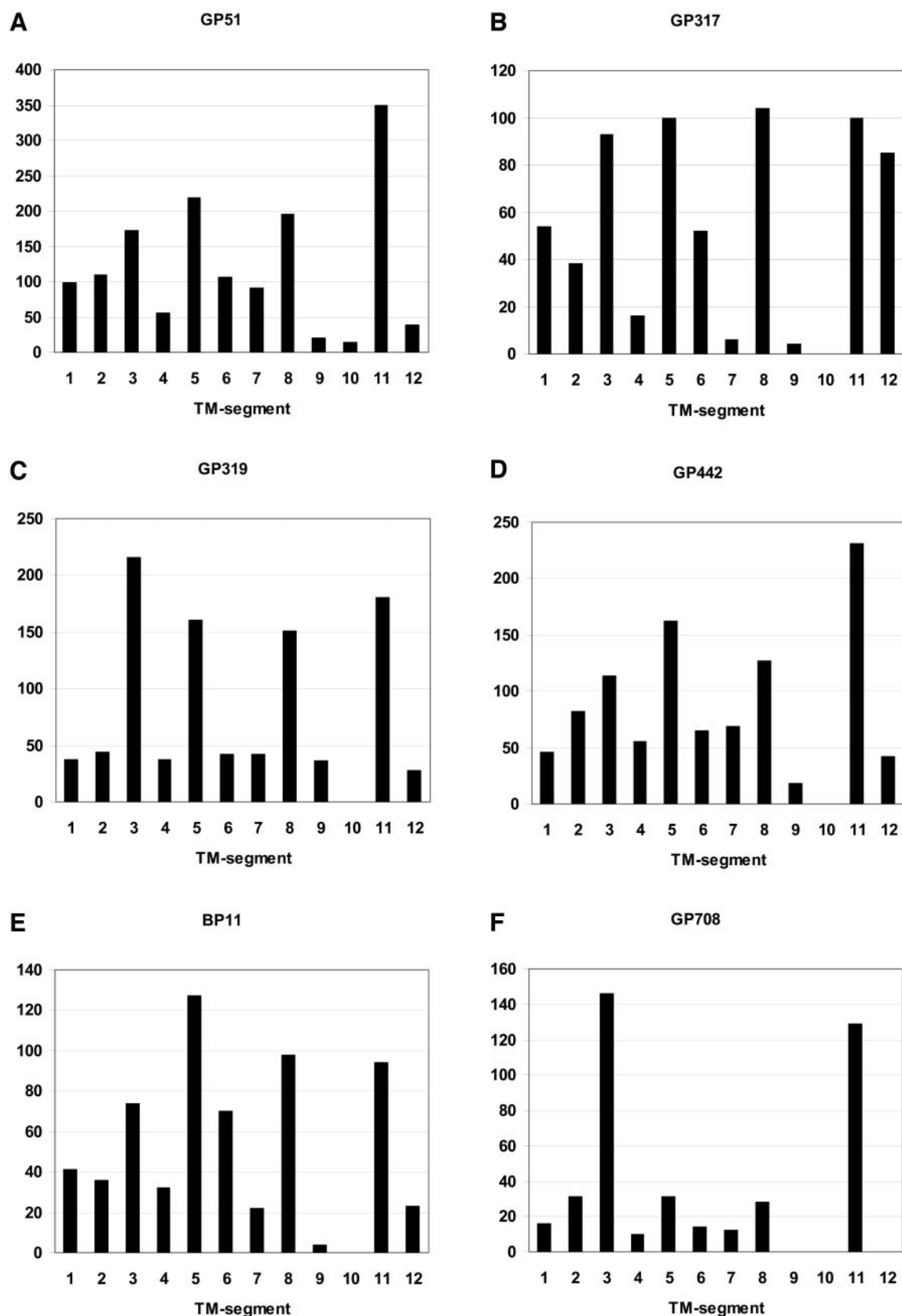


Fig. 2. Cumulative labeling frequency expressed as the area under curve for each individual ligand and TM segment. To exclude accessory surface labeling, the first three extra- and intracytoplasmic amino acid residues of each TM segments were excluded from calculations. Ordinate numbers represent the cumulative number of amino acid residues found in fragments localizing to the respective TM segment. A, ligand GPV51; B, ligand GPV317; C, ligand GPV319; D, ligand GPV442; E, ligand BP11; F, ligand GPV708. For structures of the ligands, see Table 1. The highest scores were invariably obtained for TMs 3, 5, 8, and 11 with ligands GPV51, 317, 319, 442, and BP11. GPV708 (F) only labeled TM segments 3 and 11.

ual TM segments. Strongly labeled TM segments (closed symbols) showed broad overlap with poorly labeled TMs with respect to expected fragment density. Results were therefore not biased for the probability of retrieval of peptide fragments from different TM segments.

Generation of a Three-Dimensional Atomic Detail Model of P-gp. A protein homology model of P-gp was gen-

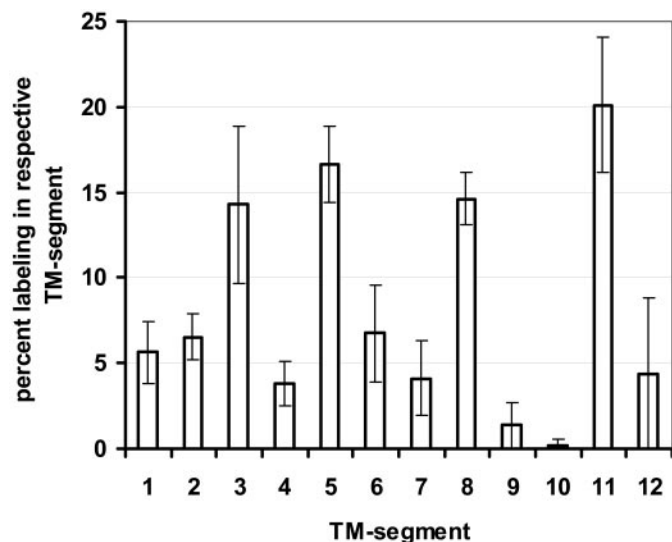


Fig. 3. Average relative labeling frequencies of the TM segments obtained with six photoligands. Mean and standard deviations are given. Because ligand GPV708 did not label TMs 5 and 8, it was excluded from calculations for these two TM helices. As for the individual ligands depicted in Fig. 2, the highest scores were obtained for TMs 3, 5, 8, and 11, and differences in labeling between each of these four TM segments and all other TM segments were statistically significant at $p < 0.001$.

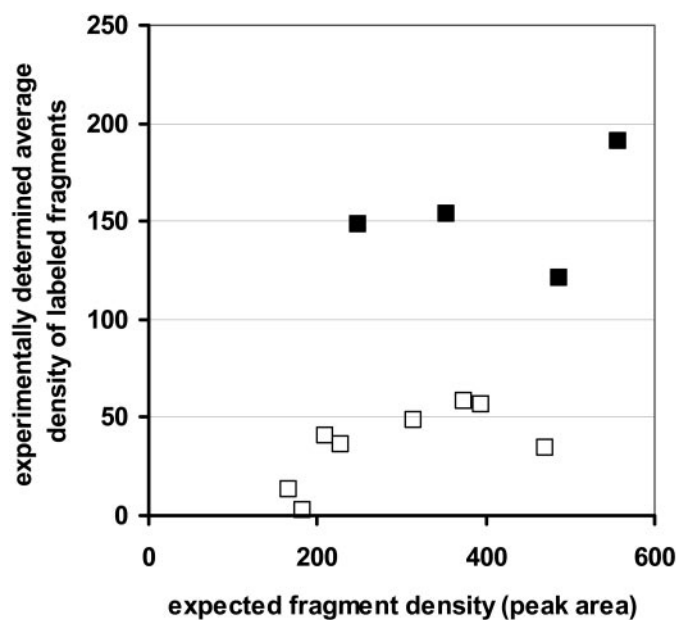


Fig. 4. Theoretical peptide fragment density for the individual TM segments of P-gp. The prediction is derived from an incomplete *in silico* digest of P-gp with chymotrypsin. Values were obtained by counting the number of amino acid residues in fragments overlapping with each individual TM segment. Expected fragment densities showed broad overlap for TM segments with high labeling (TMs 3, 5, 8, and 11, ■) and those with poor labeling (helices 1, 2, 4, 6, 7, 9, 10 and 12, □). Data indicate that photolabeling results are not biased for differences in recovery of peptide fragments from different TM segments.

erated to allow projection of labeling data on a 3D model of the protein as described in detail under *Materials and Methods*. The crystal structure of dimeric Vc-MsbA became available recently (Chang, 2003). This structure shows higher resolution than the structure of *Escherichia coli* MsbA, which has been used as a template for a previous modeling study (Stenham et al., 2003). Vc-MsbA is an essential lipid transporter, which shares structural and functional homology with P-gp as well as LmrA, an ATP-driven multidrug efflux pump from *Lactococcus lactis* (Reuter et al., 2003). The initial P-gp model (model A) is shown as a stereomage in Fig. 5. The model predicts that the TM segments form a helical bundle, which lines a central water-filled chamber with access to the extracellular space. TMs 3, 5, and 6 as well as 9, 11, and 12 are predicted to have broad access to the central cavity, whereas the access of TM segments 2 and 8 seems restricted. The TMD/TMD interfaces involve contributions of TM segments 2, 3, and 11 on one side and 5, 8, and 9 on the other side of the aqueous pore.

In contrast to the template, which lines a central cavity that is narrower at the extracytoplasmic face, P-gp has been shown to be funnel-shaped (Loo and Clarke, 2001; Rosenberg et al., 2001, 2003) with the TM segments being closer at their cytoplasmic ends than at the extracellular surface of the membrane. Therefore, the TMDs were repositioned manually by slightly moving the TMDs apart at the extracellular surface and narrowing them at the cytoplasmic face. This and subsequent recalculation of the TMD/NBD linker led to the model depicted in side and top view in Fig. 6. This model (model B) satisfied the majority of the distance constraints established by cysteine cross-linking studies better than model A. Table 2 gives a synopsis of distance constraints obtained by site-directed mutagenesis and subsequent cysteine cross-linking experiments. The table lists the positions of mutated residues and distances in models A and B. These distances are similar to those reported for a P-gp model

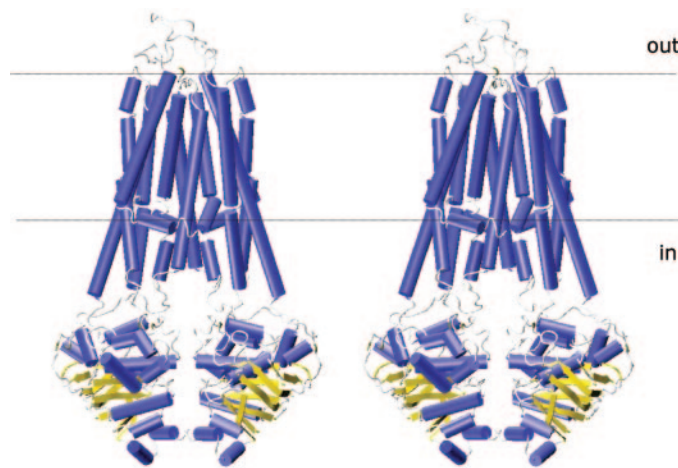


Fig. 5. Stereomage of a P-gp homology model (model A) generated on basis of the X-ray structure of Vc-MsbA. The nucleotide binding domain was modeled on the basis of the structure of TAP1 as described under *Materials and Methods*. TM segments form a helical bundle which lines a central pore that connects to the extracellular environment. TMs 1 and 7 can easily be identified by a short α helix, which lies just N-terminal and in a 90° angle relative to these TM segments. The short helix is almost parallel to the membrane and defines the approximate location of the inner membrane-water interface. The two broken horizontal lines give the approximate position of the membrane boundaries.

generated with a different template structure (*E. coli* MsbA) (Stenham et al., 2003).

Relating the Substrate Photoaffinity Labeling Information to the 3D Atomic Detail Model of P-gp. As indicated above, putative TM segments 3, 5, 8, and 11 showed highest accessibility for substrate-type photoaffinity ligands, with the peak scoring positions being Met197 in TM3, Ala311 in TM5, Thr769 in TM8, and Phe951 in TM11. These amino acid residues were displayed in the model shown in Fig. 6 with their Connolly surfaces colored in yellow and red, respectively. This revealed a number of remarkable facts. First, when looking at the stereoisimage of the side view of the model, one is able to appreciate that these residues are located at approximately the same height and predicted to be buried deep within the membrane (membrane boundaries are indicated by horizontal lines) approximately halfway between the inner and the outer membrane surface. Second, Met197 in TM3 and Phe951 in TM11 are in close vicinity of each other but are located on different halves of P-gp [the latter are depicted in dark blue (N-terminal half) and cyan (C-terminal half), respectively]. Thus, helices 3 and 11 contribute to one of the two TMD/TMD interfaces. The peak scoring residues are shown in yellow in the stereoisimage. Both the side and the top view of the P-gp model demonstrate the close spatial vicinity of these residues, which show a C_{α} -carbon distance of less than 9 Å. Third, Ala311 in TM 5 and Thr769 in TM8 are located at the other TMD/TMD interface and have a C_{α} -carbon distance of less than 14 Å. Thus, labeling data suggest the presence of two substrate-

binding domains at two pseudosymmetrical TMD/TMD interfaces formed by TM3 of the N-terminal TMD and TM11 of the C-terminal TMD and by TM5 of the N-terminal and TM8 of the C-terminal NBD. It is interesting that only one of these interfaces contains methionine residues (TM3 and TM11), whereas the other (TM5 and TM8) is methionine-free. This indicates that labeling at the domain interfaces does not depend on the presence of methionine residues. In addition, the labeling is pseudosymmetrical, because substrate binding at the TMD/TMD interfaces occurs to TM3 of the N-terminal and TM5 of the C-terminal half (corresponding to TM11) but TM2 of the C-terminal TMD (corresponding to TM8) and TM5 of the N-terminal TMD. This rotational pseudosymmetry is in agreement with the low-resolution structure of P-gp obtained by electron cryomicroscopy (Rosenberg et al., 2001, 2003) and with recent data by Loo, Bartlett, and Clarke, showing that cross-links between equivalent AA positions in TMs 2/11 and 5/8 are influenced differently by the same drug substrates (Loo et al., 2004b). In addition, ligand GPV708 only labels the interface formed by TMs 3 and 11, whereas the other interface domain is not labeled.

Discussion

The P-gp protein homology model generated in this study (Fig. 6) conforms to the majority of distance constraints obtained by previous systematic cross-linking studies of double-cysteine mutants (Table 2). In particular, the spatial proximity of TM helices 5/8 and 2/11 has been shown by two different groups (Stenham et al., 2003; Loo et al., 2004a,b). Stenham et al. replaced three consecutive amino acid residues in the extracellular halves of each, TM segments 2/11 and 5/8, to allow cross-links independent of the relative rotational positioning of these helices toward each other and showed that cross-links were indeed detected.

Loo, Bartlett, and Clarke used double-cysteine mutants in TM5/8 and 2/11, respectively (Loo et al., 2004a,b). In particular, cross-linking between Asn296 and Gly774 and Ile299 and Phe770 as well as between Ile299 and Gly774 and Gly300 and Phe300 were observed when these residues were replaced by cysteines and subsequently cross-linked with the zero-length cross-linker copper phenanthroline. With respect to putative TMs 2 and 11, cross-links were found for the double-cysteine mutants Val133/Gly939, C137C/A935C, and L138C/A935C. As in other P-gp models (Seigneuret and Garnier-Suillerot, 2003; Stenham et al., 2003) the distance between helix 2 and 11 exceeds 7 Å, the latter being the maximal distance for cross-linking of residues with the zero-length cross-linker copper phenanthroline. Despite this fact, the model depicted in Fig. 6 accurately predicts the spatial proximity of the helix pairs 5/8 and 2/11.

Loo, Bartlett, and Clarke also generated 100 TM3 to TM11 double-cysteine mutants in the inner half of these helices, but no cross-links were detected with copper phenanthroline. Consistent with these results, the model in Fig. 6 predicts helices 3 and 11 to be closer at their extracytoplasmic half, whereas they are more distant at the cytoplasmic half.

A protein homology model must be viewed as an approximation of the structure of a protein rather than as an accurate 3D structure, and the exact positioning of TM segments 2/3/11 and 5/8/9 at the TMD/TMD interfaces might be some-

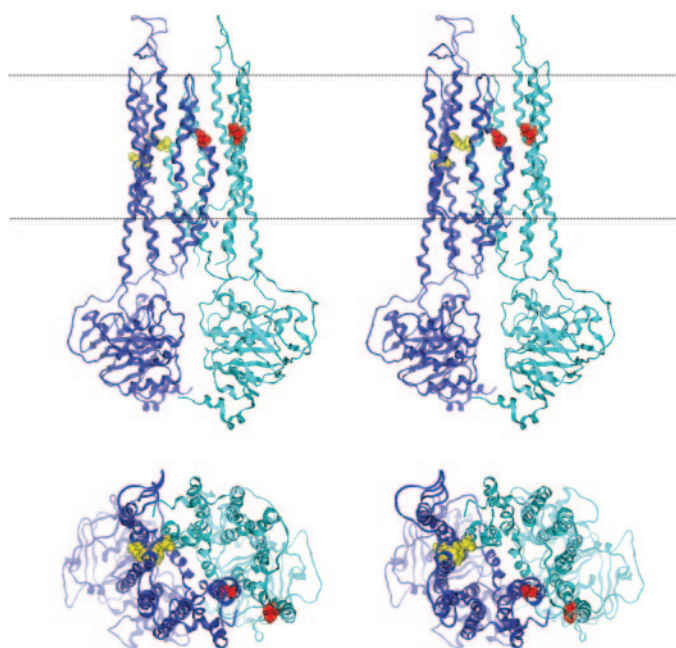


Fig. 6. Stereoisimage of a side and top view of a refined P-gp model (model B). This model was generated to account for experimental evidence that the central pore is wider at the extracytoplasmic face of the membrane than at the cytoplasmic face. The N-terminal half of P-gp is depicted in dark blue, and the C-terminal half is in cyan. Residues with the highest labeling scores are depicted in yellow (residues Met197 in TM3 and Phe951 in TM11) and red (Ala311 in TM5 and Thr769 in TM8), respectively. These residues are located at the two TMD/TMD interfaces. The two residues depicted in yellow (Met197 and Phe951) have C_{α} -carbon distances of less than 9 Å, whereas the residues depicted in red (Ala311 and Thr769) are less than 14 Å apart. The side view indicates that these four residues are located at similar depth within the membrane.

what different from that shown in our model. The symmetrical Vc-MsbA template necessarily yields a symmetrical model, although for P-gp, an asymmetry has been documented experimentally (Rosenberg et al., 2001; Loo et al., 2004b). Nevertheless, the scarcity of available membrane protein structures (as of August 2004, 82 unique membrane proteins are structurally resolved at atomic level; however, none of the resolved structures is an ATP-dependent multidrug transporter) makes these computational models particularly valuable as a starting point for the integration of photoaffinity-labeling data and 3D structure. The models are also capable of guiding the design of mutant P-gp to validate data obtained by cross-linking studies and to use these cross-links as constraints in molecular dynamics simulations.

In the present study, photoaffinity labeling allowed the identification of an involvement of four TM helices, TMs 3, 5, 8, and 11, in the primary substrate binding event. These helices are located at the TMD/TMD interfaces, and conformational changes at these interfaces might provide an explanation for why such a large number of compounds can be adopted and transported by P-gp. A schematic top view of P-gp is shown in Fig. 7. The amino- and carboxyl-terminal halves of the transporter are symbolized by blue and cyan arches. Individual helices 1 to 6 and 7 to 12 are represented in the same color but with darker shading. Relative positions and colors are identical with those in Fig. 6. The central pore is depicted in black. The pairs of helices involved in substrate binding also refer to the model in Fig. 6 and are indicated by yellow and red numbering. Arrows indicate the putative path by which substrates access their binding sites.

Binding of substrates at interfaces has been shown previously for AcrB, a proton motive force-driven multidrug efflux pump from *E. coli*, which has been cocrystallized in the presence of four substrates: ethidium, ciprofloxacin, dequalinium, and rhodamine 6G (Yu et al., 2003). We recently showed that the ATP-dependent multidrug transporter LmrA from *L. lactis* also binds substrates at the TMD/TMD interfaces (Ecker et al., 2004). Given that at least three

different multidrug transporters bind substrates at domain interfaces suggests that this might be a common property of polyspecific drug efflux pumps. The fact that a number of peptide fragments were identified to contain more than one covalently bound photoaffinity ligand suggests that, similar to AcrB and other polyspecific proteins, more than one substrate molecule can be adopted in the binding domains at a time (Neyfakh, 2002; Schumacher and Brennan, 2003). Thus, different amino acid residues in the binding sites are likely to be able to substitute for each other to accommodate structurally diverse substrate molecules. Evidence for the simultaneous binding of two different drugs in the binding pocket of P-gp has been presented previously by Loo et al. (2003). Acceptance or exclusion of substrates on the basis of defined physicochemical parameters such as π - π , hydrophobic, and dipolar interactions (Chiba et al., 1995; Ecker et al., 1999; Seelig and Landwojtowicz, 2000), together with the plasticity of the TMD/TMD interfaces, might be the underlying principle of multispecificity. For the regulatory proteins BmrR of *Bacillus subtilis* and QacR, a repressor from *Staphylococcus aureus*, X-ray studies in complex with ligands have demonstrated binding in rather large binding pockets (Schumacher and Brennan, 2003). The binding was mediated mostly by hydrophobic interactions, with key electrostatic contributions from glutamic acid residues. The latter can be ruled out for substrate P-gp interaction, because TM segments do not contain charged amino acid residues. However, dipolar interactions might substitute for electrostatic interactions. In the apolar environment of the membrane, stable hydrogen bonds can be formed, and ligand-based design has shown that hydrogen bonding properties contribute to the binding of propafenone analogs (Chiba et al., 1995) and other substance groups (Seelig and Landwojtowicz, 2000). It is interesting that the protonable nitrogen atom in propafenones contributes to biological activity by its hydrogen bonding and not by its electrostatic properties (Ecker et al., 1999).

For multispecific proteins, loose binding pockets are able to accommodate more than one ligand at the same time, whereby different orientations for one and the same ligand are possible. Our results indicate that this also applies for P-gp. A number of peptide fragments contain two covalently bound ligands, suggesting the simultaneous presence of more than one substrate molecule in the binding pocket. This necessitates the notion of different but coexisting substrate orientations.

The random nature of ATP hydrolysis in one of two nucleotide binding sites has been shown (Ambudkar et al., 2003; Al-Shawi et al., 2003); whether substrate binding also follows random characteristics is unclear. Our findings are compatible with both binding of substrates to one P-gp molecule at two sites in random manner or simultaneous binding at both binding domains. It is interesting that ligand GPV708 only labels the TM 3/11 interface and thus clearly binds in non-random manner, providing a proof of principle for a pairwise contribution of TM segments 3/11 and 5/8 to two binding domains.

In conclusion, our study provides evidence that substrates access the central cavity of P-gp via the TMD/TMD interfaces and that these interfaces are asymmetric with respect to the contribution of TM helices in the two halves of P-gp. Photoligands used in this study combine the advantage of well-defined quantitative structure-activity relationships and an

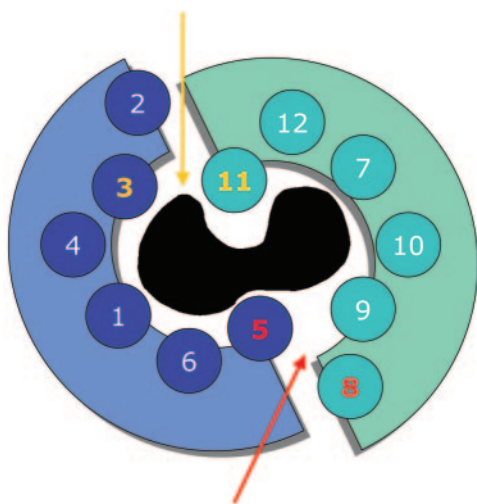


Fig. 7. Schematic representation of a top view of P-gp. The N- and C-terminal halves are symbolized by dark blue and cyan arches, respectively. Circles and numbers indicate the TM segments. Labeled TMs are numbered in yellow and red. These helices are located at the two TMD/TMD interfaces. The red and yellow arrows symbolize the path along which substrates are believed to access their binding sites. See Discussion for details.

unmodified core structure compared with propafenone. This motivated sole use of these compounds in the present study. Nevertheless, heterologous displacement studies with known P-gp substrates indicate the general nature of our results extending to other substance classes. Future studies will be directed at identifying possible changes in the labeling pattern at different steps of the catalytic cycle of P-gp. These studies might allow the evolution of a concept that links P-gp structure to the dynamics of the transport process.

Acknowledgments

The baculovirus expression vector pVL941-MDR1/A was generously provided by Dr. M. M. Gottesman (National Cancer Institute, Bethesda, MD). The technical assistance of F.C. and N.C. during July 2004 is greatly appreciated.

References

- Al-Shawi MK, Polar MK, Omote H, and Figler RA (2003) Transition state analysis of the coupling of drug transport to ATP hydrolysis by P-glycoprotein. *J Biol Chem* **278**:52629–52640.
- Ambudkar SV, Kimchi-Sarfaty C, Sauna ZE, and Gottesman MM (2003) P-glycoprotein: from genomics to mechanism. *Oncogene* **22**:7468–7485.
- Chang G (2003) Structure of MsbA from *Vibrio cholera*: a multidrug resistance ABC transporter homolog in a closed conformation. *J Mol Biol* **330**:419–430.
- Chiba P, Burghofer S, Richter E, Tell B, Moser A, and Ecker G (1995) Synthesis, pharmacologic activity and structure-activity relationships of a series of propafenone-related modulators of multidrug resistance. *J Med Chem* **38**:2789–2793.
- Chiba P, Ecker G, Schmid D, Drach J, Tell B, Goldenberg S, and Gekeler V (1996) Structural requirements for activity of propafenone-type modulators in P-glycoprotein-mediated multidrug resistance. *Mol Pharmacol* **96**:1122–1130.
- Clauser KR, Baker PR, and Burlingame AL (1999) Role of accurate mass measurements (± 10 ppm) in protein identification strategies employing MS or MS/MS and database searching. *Anal Chem* **71**:2871–2882.
- Dorman G and Prestwich GD (2000) Using photolabile ligands in drug discovery and development. *Trends Biotechnol* **18**:64–77.
- Ecker G, Csaszar E, Kopp S, Plagens B, Holzer W, Ernst W, and Chiba P (2002) Identification of ligand-binding regions of P-glycoprotein by activated-pharmacophore photoaffinity labeling and matrix-assisted laser desorption/ionization-time of flight mass spectrometry. *Mol Pharmacol* **61**:637–648.
- Ecker G, Huber M, Schmid D, and Chiba P (1999) The importance of a nitrogen atom in modulators of multidrug resistance. *Mol Pharmacol* **56**:791–796.
- Ecker GF, Pleban K, Kopp S, Csaszar E, Poelarends GJ, Putman M, Kaiser D, Konings WN, and Chiba P (2004) A three dimensional model for the substrate binding domain of the multidrug ABC transporter LmrA. *Mol Pharmacol* **66**:1169–1179.
- Germann UA, Willingham MC, Pastan I, and Gottesman MM (1990) Expression of the human multidrug transporter in insect cells by a recombinant baculovirus. *Biochemistry* **29**:2295–2303.
- Hafkemeyer P, Dey S, Ambudkar SV, Hrycyna CA, Pastan I, and Gottesman MM (1998) Contribution to substrate specificity and transport of nonconserved residues in transmembrane domain 12 of human P-glycoprotein. *Biochemistry* **37**:16400–16409.
- Humphrey W, Dalke A, and Schulten K (1996) VMD: visual molecular dynamics. *J Mol Graph* **14**:33–38, 27–28.
- Loo TW and Clarke DM (2000) The packing of the transmembrane segments of human multidrug resistance P-glycoprotein is revealed by disulfide cross-linking analysis. *J Biol Chem* **275**:5253–5256.
- Loo TW and Clarke DM (2001) Determining the dimensions of the drug-binding domain of human P-glycoprotein using thiol cross-linking compounds as molecular rulers. *J Biol Chem* **276**:36877–36880.
- Loo TW, Bartlett MC, and Clarke DM (2003) Simultaneous binding of two different drugs in the binding pocket of the human multidrug resistance P-glycoprotein. *J Biol Chem* **278**:39706–39710.
- Loo TW, Bartlett MC, and Clarke DM (2004a) Disulfide cross-linking analysis shows that transmembrane segments 5 and 8 of human P-glycoprotein are close together on the cytoplasmic side of the membrane. *J Biol Chem* **279**:7692–7697.
- Loo TW, Bartlett MC, and Clarke DM (2004b) Val133 and Cys137 in transmembrane segment 2 are close to Arg935 and Gly939 in transmembrane segment 11 of human P-glycoprotein. *J Biol Chem* **279**:18232–18238.
- Neyfakh AA (2002) Mystery of multidrug transporters: the answer can be simple. *Mol Microbiol* **44**:1123–1130.
- Peer M, Csaszar E, Vorlauffer E, Kopp S, and Chiba P (2004) Photoaffinity labeling of P-glycoprotein. *Mini Rev Med Chem*, in press.
- Reuter G, Janvilisri T, Venter H, Shahi S, Balakrishnan L, and van Veen HW (2003) The ATP binding cassette multidrug transporter LmrA and lipid transporter MsbA have overlapping substrate specificities. *J Biol Chem* **278**:35193–35198.
- Rihakova L, Deraet M, Auger-Messier M, Perodin J, Boucard AA, Guilemette G, Leduc R, Lavigne P, and Escher E (2002) Methionine proximity assay, a novel method for exploring peptide ligand-receptor interaction. *J Recept Signal Transduct Res* **22**:297–313.
- Rosenberg MF, Kamis AB, Callaghan R, Higgins CF, and Ford RC (2003) Three-dimensional structures of the mammalian multidrug resistance P-glycoprotein demonstrate major conformational changes in the transmembrane domains upon nucleotide binding. *J Biol Chem* **278**:8294–8299.
- Rosenberg MF, Velarde G, Ford RC, Martin C, Berridge G, Kerr ID, Callaghan R, Schmidlin A, Wooding C, Linton KJ, et al. (2001) Repacking of the transmembrane domains of P-glycoprotein during the transport ATPase cycle. *EMBO (Eur Mol Biol Organ) J* **20**:5615–5625.
- Sauna ZE and Ambudkar SV (2000) Evidence for a requirement for ATP hydrolysis at two distinct steps during a single turnover of the catalytic cycle of human P-glycoprotein. *Proc Natl Acad Sci USA* **97**:2515–2520.
- Sauna ZE and Ambudkar SV (2001) Characterization of the catalytic cycle of ATP hydrolysis by human P-glycoprotein. *J Biol Chem* **276**:11653–11661.
- Schmid D, Ecker G, Kopp S, Hitzler M, and Chiba P (1999) Structure-activity relationship studies of propafenone analogs based on P-glycoprotein ATPase activity measurements. *Biochem Pharmacol* **58**:1447–1456.
- Schumacher MA and Brennan RG (2003) Deciphering the molecular basis of multidrug recognition: crystal structures of the *Staphylococcus aureus* multidrug binding transcription regulator QacR. *Res Microbiol* **154**:69–77.
- Seelig A and Landwojtowicz E (2000) Structure-activity relationship of P-glycoprotein substrates and modifiers. *Eur J Pharm Sci* **12**:31–40.
- Seigneuret M and Garnier-Suillerot A (2003) A structural model for the open conformation of the mdr1 P-glycoprotein based on the MsbA crystal structure. *J Biol Chem* **278**:30115–30124.
- Senior AE and Gadsby DC (1997) ATP hydrolysis cycles and mechanism in P-glycoprotein and CFTR. *Semin Cancer Biol* **8**:143–150.
- Stenham DR, Campbell JD, Sansom MS, Higgins CF, Kerr ID, and Linton KJ (2003) An atomic detail model for the human ATP binding cassette transporter P-glycoprotein derived from disulfide cross-linking and homology modeling. *FASEB J* **17**:2287–2289.
- Wahlstrom JL, Randall MA, Lawson JD, Lyons DE, Siems WF, Crouch GJ, Barr R, Facemyer KC, and Cremo CR (2002) Structural model of the regulatory domain of smooth muscle heavy meromyosin. *J Biol Chem* **278**:5123–5131.
- Yu EW, Aires JR, and Nikaido H (2002) AcrB multidrug efflux pump of *Escherichia coli*: composite substrate-binding cavity of exceptional flexibility generates its extremely wide substrate specificity. *J Bacteriol* **185**:5657–5664.
- Yu EW, McDermott G, Zgurskaya HI, Nikaido H, and Koshland DE Jr (2003) Structural basis of multiple drug-binding capacity of the AcrB multidrug efflux pump. *Science (Wash DC)* **300**:976–980.

Address correspondence to: Dr. Peter Chiba, Institute of Medical Chemistry, Medical University of Vienna, Währingerstrasse 10, A-1090 Vienna, Austria. E-mail: peter.chiba@meduniwien.ac.at